Higher-Order Photon Bunching in a Semiconductor Microcavity

M. Aßmann, *et al.*

Science **325**, 297 (2009);
DOI: 10.1126/science.1174488

the maximal resistance does not match the theoretical value obtained from Eqs. 1 and 2, but still remains an integer fraction of the quantum h/e^2. This result can be naturally understood as due to inhomogeneities in the gate action (e.g., due to interface trap states) inducing some metallic droplets close to the edge channels while the bulk of the sample is insulating. A metallic droplet can cause dephasing of the electronic wave function, leading to fluctuations in the device resistance. For full dephasing, the droplet plays the role of an additional ohmic contact, just as for the chiral edge channels in the QH regime (*8*). More details on the effects of additional ohmic contacts in the QSH state are given in (*11*).

Another measurement that directly confirms the nonlocal character of the helical edge channel transport in the QSH regime is in Fig. 4, which shows data obtained from device D4, in the shape of the letter H. In this four-terminal device, the current is passed through contacts 1 and 4 and the voltage is measured between contacts 2 and 3. In the metallic n-type regime (low gate voltage), the voltage signal tends to zero. In the insulating regime, however, the nonlocal resistance signal increases to ~6.5 kilohms, which again fits perfectly to the result of Laudauer-Büttiker considerations: $R_{14,23} = h/4e^2 \approx 6.45$ kilohms. Classically, one would expect only a minimal signal in this configuration (from Poisson's equation, assuming diffusive transport, one estimates a signal of about 40 ohms), and certainly not one that increases so strongly when the bulk of the sample is depleted. This signal measured here is fully nonlocal and can be taken (as was done 20 years ago for the QH regime) as definite evidence of the existence of edge channel transport in the QSH regime. A similar nonlocal voltage has been studied in a metallic spin Hall system with the same H-bar geometry (*12*), in which case the nonlocal voltage can be understood as a combination of the spin Hall effect and the inverse spin Hall effect (*13*). The quantized nonlocal resistance $h/4e^2$ we find here is the quantum counterpart of the metallic case. For example, if we assume that the chemical potential in contact 1 is higher than that in contact 4 (compare to the layout of D4 in Fig. 2B), more electrons will be injected into the upper edge state in the horizontal segment of the H-bar than into the lower edge state. Because on opposite edges the right-propagating edge states have opposite spin, this implies that a spin-polarized current is generated by an applied bias $V_1 - V_4$, comparable to a spin Hall effect. When this spin-polarized current is injected into the right leg of the device, the inverse effect occurs. Electrons in the upper edge flow to contact 2 while those in the lower edge flow to contact 3, establishing a voltage difference between those two contacts due to the charge imbalance between the edges. The right leg of the device thus acts as a detector for the injected spin-polarized current, which corresponds to the inverse spin Hall effect.

Concluding remarks. The multiterminal and nonlocal transport experiments on HgTe microstructures in the QSH regime demonstrate that charge transport occurs through extended helical edge channels. We have extended the Landauer-Büttiker model for multiterminal transport in the QH regime to the case of helical QSH edge channels and have shown that this model convincingly explains the observations. Logic devices based on the complementary metal oxide semiconductor design generate considerable heating due to the ohmic dissipation within the channel. Our work on conductance quantization demonstrates that electrons can be transported coherently within the edge channel without ohmic dissipation. Such an effect can be used to construct logic devices with improved performance.

References and Notes

1. S. C. Zhang, *Physics* **1**, 6 (2008).
2. C. L. Kane, E. J. Mele, *Phys. Rev. Lett.* **95**, 226801 (2005).
3. B. A. Bernevig, S. C. Zhang, *Phys. Rev. Lett.* **96**, 106802 (2006).
4. C. Wu, B. A. Bernevig, S. C. Zhang, *Phys. Rev. Lett.* **96**, 106401 (2006).
5. C. Xu, J. Moore, *Phys. Rev. B* **73**, 045322 (2006).
6. B. A. Bernevig, T. L. Hughes, S.-C. Zhang, *Science* **314**, 1757 (2006).
7. M. König *et al.*, *Science* **318**, 766 (2007); published online 19 September 2007 (10.1126/science.1148047).
8. C. W. J. Beenakker, H. van Houten, *Solid State Phys.* **44**, 1 (1991).
9. M. Büttiker, *Phys. Rev. B* **38**, 9375 (1988).
10. M. Büttiker, *Phys. Rev. Lett.* **57**, 1761 (1986).
11. See supporting material on *Science* Online.
12. C. Brüne *et al.*, http://arxiv.org/abs/0812.3768 (2008).
13. E. M. Hankiewicz, L. W. Molenkamp, T. Jungwirth, J. Sinova, *Phys. Rev. B* **70**, 241301(R) (2004).

14. We thank T. Beringer, N. Eikenberg, M. König, and S. Wiedmann for assistance in some of the experiments. Supported by Deutsche Forschungsgemeinschaft grant SFB 410; German-Israeli Foundation grant I-881-138.7/2005; NSF grant DMR-0342832; the Alexander von Humboldt Foundation; the U.S. Department of Energy, Office of Basic Energy Sciences, under contract DE-AC03-76SF00515; the Focus Center Research Program (FCRP) Center on Functional Engineered Nanoarchitectonics; the National Science and Engineering Research Council of Canada; and the Stanford Graduate Fellowship Program. Computational work was made possible by the facilities of the Shared Hierarchical Academic Research Computing Network (www.sharcnet.ca).

Supporting Online Material

www.sciencemag.org/cgi/content/full/325/5938/294/DC1
SOM Text
Figs. S1 to S9
Table S1
References

8 April 2009; accepted 11 June 2009
10.1126/science.1174736

Higher-Order Photon Bunching in a Semiconductor Microcavity

M. Aßmann,[1] F. Veit,[1] M. Bayer,[1]* M. van der Poel,[2] J. M. Hvam[2]

Quantum mechanically indistinguishable particles such as photons may show collective behavior. Therefore, an appropriate description of a light field must consider the properties of an assembly of photons instead of independent particles. We have studied multiphoton correlations up to fourth order in the single-mode emission of a semiconductor microcavity in the weak and strong coupling regimes. The counting statistics of single photons were recorded with picosecond time resolution, allowing quantitative measurement of the few-photon bunching inside light pulses. Our results show bunching behavior in the strong coupling case, which vanishes in the weak coupling regime as the cavity starts lasing. In particular, we verify the *n* factorial prediction for the zero-delay correlation function of *n* thermal light photons.

The discovery of two-photon bunching in thermal light by Hanbury Brown and Twiss (*1*) marked a turning point for the development of quantum optics (*2*) and has also found applications in a variety of fields, from particle physics (*3*) to ultracold quantum gases (*4*). Photon bunching is the tendency of indistinguishable photons, emitted by a thermal or chaotic light source, to show an enhanced joint detection probability compared with statistically independent particles that are emitted, for instance, by lasers. The explanation of this bunching relies on quantum interference between indistinguishable *n* particle probability amplitudes leading to excess joint detections if the photon number follows the Bose-Einstein distribution (*5*, *6*).

The quantity describing bunching for two photons is the second-order intensity correlation function defined as

$$g^{(2)}(t,\tau) = \frac{\langle :\hat{n}(t)\hat{n}(t+\tau): \rangle}{\langle \hat{n}(t) \rangle \langle \hat{n}(t+\tau) \rangle} \qquad (1)$$

where $\hat{n} = \hat{a}^{\dagger}\hat{a}$ is the photon number operator, t and $t + \tau$ are the detection times of the two

[1]Experimentelle Physik II, Technische Universität Dortmund, D-44221 Dortmund, Germany. [2]DTU Fotonik, Technical University of Denmark, DK-2800 Kongens Lyngby, Denmark.

*To whom correspondence should be addressed: E-mail: manfred.bayer@tu-dortmund.de

photons, and the double stops denote normal and apex ordering of the underlying photon creation and annihilation operators $\hat{a}^{\dagger}$ and $\hat{a}$. This normal ordering accounts for the change of the light field by the detection of a photon (i.e., when one photon is destroyed). $g^{(2)}(t,\tau)$ gives the average value of joint detections normalized by the product of the average photon numbers at times t and $t+\tau$. The latter is the number of joint detections one would expect if the photons were statistically independent particles. In particular, the equal time correlation function $g^{(2)}(t,0)$ is a direct quantitative measure of the joint detection probability.

Bunching is not limited to two-particle probability amplitudes, but it can be extended to the interference of n particle probability amplitudes. The second-order correlation function can be extended to arbitrary higher orders, thereby providing the most complete characterization of the light field possible (*7*). The nth-order correlation function is the average value of the joint detections of n photons at times t_i (where $i = 1,\ldots,n$) divided by the average photon numbers at the respective times

$$g^{(n)}(t_1 \ldots t_n) = \frac{\left\langle :\prod_{i=1}^{n} \hat{n}(t_i): \right\rangle}{\prod_{i=1}^{n} \langle \hat{n}(t_i) \rangle} \qquad (2)$$

Because of the factorial increase of possible permutations of amplitudes with increasing n for indistinguishable photons, bunching is expected to be even more prominent in higher orders: The increase of the equal time joint detection probability of n indistinguishable photons compared with the case of statistically independent particles is predicted to follow an n factorial dependence (*8*). In this general form, the definition applies to stationary light fields as well as to pulsed light fields. The only difference is that the average in $g^{(n)}$ denotes a time average in the stationary case, whereas it is an average over an ensemble of equal pulses in the nonstationary case. We will focus on equal time correlations; that is, all t_i in the definition of $g^{(n)}$ are the same, and we average over all times t. We will refer to this fixture as $g^{(n)}(\tau = 0)$.

However, photons are only indistinguishable if the delays between their emission times do not exceed the coherence time. For larger delays, photon distinguishability switches the photon number distribution to a Poissonian one, which is the distribution of statistically independent particles. In this case, no bunching will occur, and $g^{(n)}(\tau = 0)$ will equal 1 for all orders of n.

Usual schemes for measuring photon bunching need precise alignment of n separate detectors and suffer from insufficient time resolution to measure the real $g^{(n)}(\tau = 0)$ (*9*), as the coherence time is on the order of picoseconds (*10*). Additionally, most of these schemes are only suitable for stationary light fields or measure the joint detections without any normalization (*11*) or consecutive photon pairs (*12*). In all of these cases, one needs to make assumptions about $g^{(n)}(\tau = 0)$ to reconstruct it (*13*). It is therefore desirable to be able to access photon bunching directly on short time scales.

Here we studied $g^{(n)}(\tau = 0)$ of photons from the radiative decay of microcavity polaritons. At low densities, microcavity polaritons can be considered as bosons, which are created by the strong coupling of photons confined in a cavity to excitons confined in a semiconductor quantum well. The resulting composite boson is of a mixed excitonic and photonic nature. Accordingly, the far field emission of the microcavity gives information about the coherence properties of the polaritons as the emitted photons are a part of the polaritonic wave function (*14*). As a consequence of their steep dispersion, polaritons have a small effective mass leading to a low density of states and also to a high-state occupancy, which is a prerequisite for efficient demonstration of photon bunching of a single mode. Unfortunately, the small effective mass also results in a short lifetime of the polaritons, on the picosecond scale. The coherence time is expected to be on the order of picoseconds, which is much shorter than the time needed to reach thermal equilibrium with the lattice. Nevertheless, in a regime where the ground state is populated dominantly by direct carrier scattering and polariton-polariton scattering is suppressed, one can still achieve emission with thermal characteristics [supporting online material (SOM) text (*15*)].

In this regime, one expects the microcavity to be a chaotic light source with $g^{(n)}(\tau = 0) = n!$. Under high excitation power, polaritons no longer follow the model of weakly interacting bosons because of the fermionic nature of electrons and holes. Coulomb interactions play a pronounced role with increasing polariton density and manifest as a substantial blue shift of the lower polariton (LP) branch up to the point where the strong coupling regime is bleached. The microcavity turns into a vertical cavity surface-emitting laser, where population inversion and, thus, conventional photon lasing occurs. In this regime, one expects $g^{(n)}(\tau = 0) = 1$ for all orders of n.

We present experimental results of a photon-bunching measurement scheme using a streak camera, which directly measures all orders of $g^{(n)}(\tau = 0)$ within a light pulse with a time resolution sufficient for semiconductor light sources. We use a redesigned streak camera, in which the

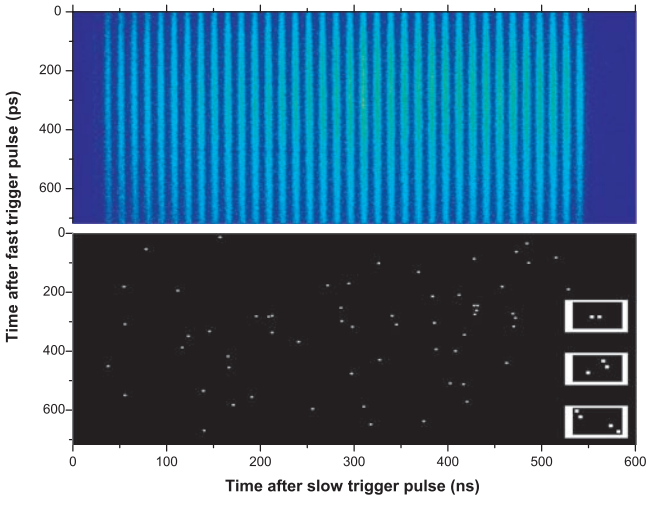

Fig. 1. Integrated intensity of 200,000 pictures compared with a single snapshot. (**Insets**) Exemplaric enlarged binning areas of 10 ps containing two-, three-, and four-photon combinations.

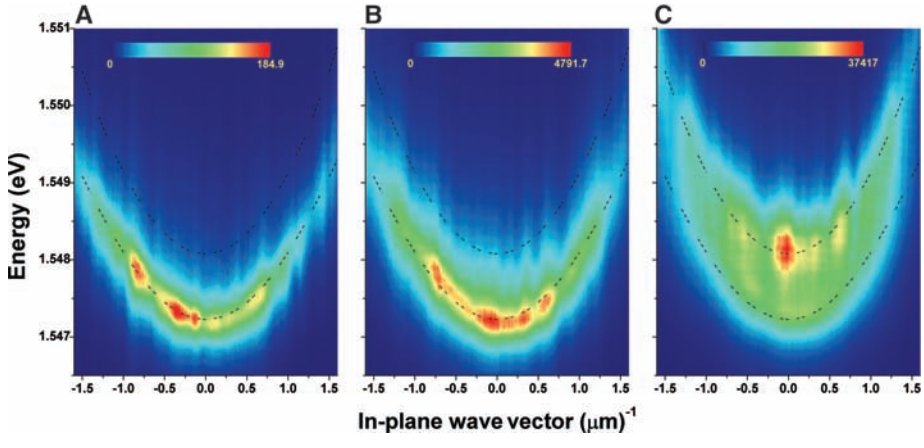

Fig. 2. Momentum distribution of the polaritons as measured by angle-resolved photoluminescence for three different excitation densities: (**A**) 50 μW (far below the lasing threshold), (**B**) 1.5 mW (at the lasing threshold), and (**C**) 10 mW (above threshold). The false color scale is linear. The black dashed lines indicate the dispersion of the LP and the bare cavity mode.

photons hit a photocathode and are converted into photoelectrons. These photoelectrons are then accelerated by time-dependent voltages and hit a phosphorus screen. Single pictures of the afterglow of this screen are recorded by a charge-coupled device's (CCD) camera. Because of the precisely controllable ramp voltage, the vertical position of the electron hitting the phosphorus screen is a direct measure of the arrival time of the photon with picosecond time resolution. Another slow, horizontal ramp voltage allows us to record the emission after several pulsed excitations on one screen, with the horizontal position of the photon hitting the phosphorus screen enabling us to distinguish between different pulses. Then pixel binning is performed. The horizontal width of the binning area is determined by the pulse width on the CCD. The vertical length of the binning area determines the time window considered as simultaneous and, therefore, also the time resolution of the system. In this case, we chose a time window of 10 ps. To determine $g^{(n)}(\tau = 0)$ from the experimental data, we count all n-photon combinations in the single pulses and divide this value by the expected number of n-photon combinations, which is the product of the averaged intensities at n times. The averaged intensity is easily accessible by summing up all single pictures; we do not need to make any additional assumptions. The results are directly derived from the measured data sets. A single screen compared with the integrated intensity of all screens is shown in Fig. 1. The insets show some binning areas containing two-, three-, and four-photon combinations. See the SOM for further technical details on the experimental setup.

The sample we studied consists of a GaAs/AlGaAs microcavity grown by molecular beam epitaxy. It contains one 10-nm-wide quantum well placed in the electric field antinode of a slightly wedged λ cavity especially designed to avoid charge accumulation in the quantum well (here, λ is the wavelength of the light confined in the cavity) (*16*). The sample displays a vacuum Rabi splitting of 3.9 meV. The polariton dispersion for different excitation densities (Fig. 2) shows an apparent bleaching of the strong coupling regime with increasing excitation power. Additionally, we found the LP ground state to be only weakly populated far below the lasing threshold. Therefore, polariton-polariton scattering is also weak in this regime. We investigated the far-field emission of the LP branch at a negative detuning of –2 meV. The Fourier plane of the emission was either imaged onto the entrance slit of a monochromator for measuring the dispersion or onto the entrance slit of a streak camera for photon counting measurements. Photons, which are emitted at an angle of θ, directly correspond to polaritons with energy E and in-plane wave vector of $k_{\parallel} = \frac{E}{\hbar c}\sin\theta$ (where $\hbar$ is Planck's constant h divided by 2π and c is the speed of light). Thus, in the first case, the entrance slit of the monochromator selects a narrow stripe with $k_{x,\parallel} = 0$. In the second case, only the $k_{\parallel} = 0$ state of the LP branch is selected with an angular resolution of ~1° by using a pinhole. Additionally, an interference filter with a 1-nm width is used to ensure that only a single mode contributes to the signal. With increasing excitation density, the filter is tuned so that the central transmission wavelength follows the blue shift of the polariton dispersion as shown in Fig. 3.

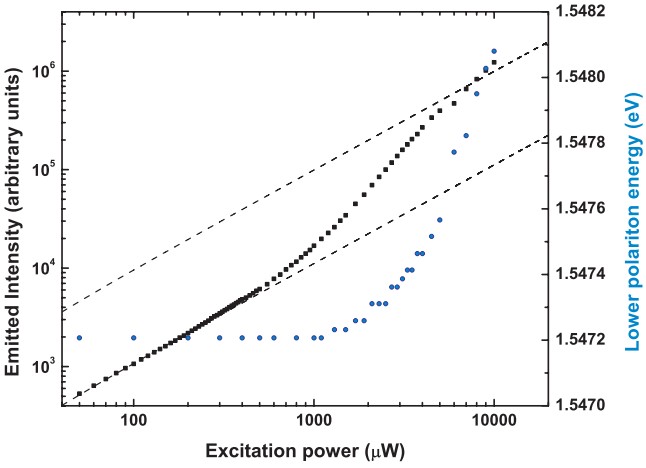

Fig. 3. Black squares indicate integrated intensity of the lasing mode measured at normal incidence as a function of the nonresonant excitation power at a detuning of −2 meV. Blue circles represent emission energy around normal incidence as a function of the excitation energy. Dashed lines indicate the linear dependence of the emitted intensity on the excitation power below (lower curve) and above (upper curve) the lasing threshold.

The measured time-averaged normalized intensity correlation functions $g^{(n)}(\tau = 0)$ up to the fourth order (Fig. 4) show that, for high excitation densities, all orders approach the expected value of 1, denoting conventional photon lasing. With decreasing excitation density, a smooth transition toward the thermal regime occurs, which is accompanied by photon bunching. At an excitation power of ~1.5 mW, the bunching effect saturates at values of approximately 2 and 6, which are the expected values of n factorial for the second and third orders of $g^{(n)}(\tau = 0)$. The fourth order also shows an increase of the joint detections, but the number of detected four-photon combinations is too small at low excitation densities to give statistically significant results in the thermal light regime. The results for different orders of $g^{(n)}(\tau = 0)$ at the same excitation power are derived from the same data set.

To assure that we measured single-mode thermal emission from the $k_{\parallel} = 0$ state, we also increased the collection angle by opening the pinhole. By doing so, we increase the number of modes contributing to the signal and, therefore, leave the regime of indistinguishable photons. As can be seen in the right inset of Fig. 4, photon bunching is only present at collection angles below 1.5°, suggesting that we are indeed operating in the single-mode thermal regime. To further ensure that our experimental results are the result of photon bunching and not just a consequence of some dominating noise source when the signal gets weaker, we also studied the blue shift of the LP and the input-output curve of the microcavity, as

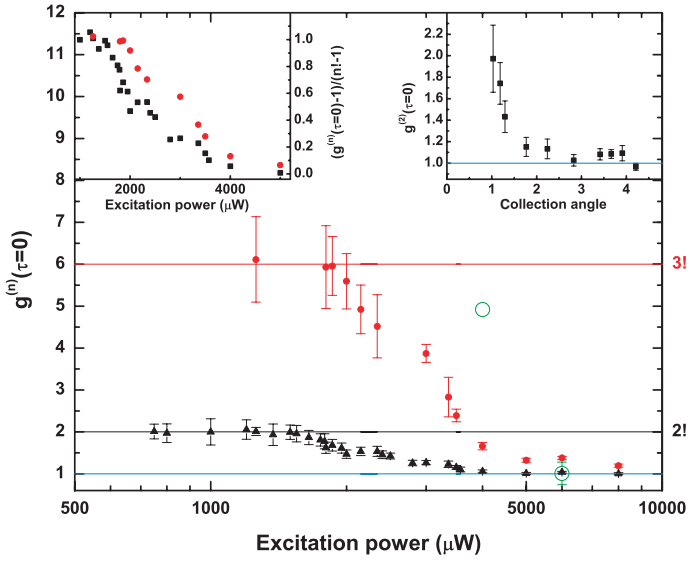

Fig. 4. Second- (black triangles), third- (red spheres), and fourth-order (green open circles) intensity correlation function versus excitation power. (**Left inset**) Close-up of the second- and third-order intensity correlation on a normalized linear scale. A value of 0 corresponds to $g^{(n)}(\tau = 0) = 1$, and a value of 1 corresponds to $g^{(n)}(\tau = 0) = n!$. (**Right inset**) Second-order intensity correlation function in the thermal regime for several total collection angles. Error bars indicate the variation of the correlations, resulting from the SDs of the detected photon numbers used for calculating $g^{(2)}$ and $g^{(3)}$.

shown in Fig. 3. The onset of the decrease of $g^{(n)}(\tau = 0)$ coincides with the beginning of the LP blue shift and the onset of a nonlinear increase in the input-output curve. This shows that the system leaves the strong coupling regime and starts to lase. At high excitation powers, well-defined lasing at the bare cavity mode builds up as expected (Fig. 2). It is obvious that the thresholds, where the $g^{(n)}(\tau = 0)$ begin to decrease toward a value of 1, do not occur at the same excitation density. This shift can be explained in terms of the low photon numbers inside the cavity at the lasing threshold. Stimulated emission sets in at a mean photon number p of the order of unity inside the mode of interest, but in the threshold region, there is still a superposition of thermal and stimulated emission present. Because of the stronger photon number fluctuations in chaotic fields, their contribution to n-photon combinations will still be substantial, whereas p is smaller than n.

Our results verify that, under nonresonant excitation, the ground state of a semiconductor microcavity in the strong coupling regime is a single-mode thermal light source and shows particularly pronounced bunching effects, even in higher orders. In terms of applications, our findings are promising for applications in quantum-optical coherence tomography or ghost imaging optics and allow for thermal light imaging, offering high temporal resolution and massively improved sensitivity for n-photon processes as compared with coherent light. From a more fundamental point of view, the demonstrated experimental technique is a versatile tool for studying quantum fluctuations and phase transitions and might especially provide further insight into the intensely debated physics of polariton lasers and the spontaneous phase transition toward polariton Bose-Einstein condensates (*17*).

References and Notes

1. R. Hanbury Brown, R. Q. Twiss, *Nature* **177**, 27 (1956).
2. F. T. Arecchi, E. Gatti, A. Sona, *Phys. Lett.* **20**, 27 (1966).
3. G. Baym, *Act. Phys. Pol. B* **29**, 1839 (1998).
4. S. Fölling *et al.*, *Nature* **434**, 481 (2005).
5. U. Fano, *Am. J. Phys.* **29**, 539 (1961).
6. G. Scarcelli, V. Berardi, Y. Shih, *Phys. Rev. Lett.* **96**, 063602 (2006).
7. U. M. Titulaer, R. J. Glauber, *Phys. Rev.* **140**, B676 (1965).
8. G. S. Agarwal, *Phys. Rev. A* **1**, 1445 (1970).
9. B. L. Morgan, L. Mandel, *Phys. Rev. Lett.* **16**, 1012 (1966).
10. S. M. Ulrich *et al.*, *Phys. Rev. Lett.* **98**, 043906 (2007).
11. P. Michler *et al.*, *Science* **290**, 2282 (2000).
12. J. Kasprzak *et al.*, *Phys. Rev. Lett.* **100**, 067402 (2008).
13. D. M. McAlister, M. G. Raymer, *Phys. Rev. A* **55**, R1609 (1997).
14. V. Savona, F. Tassone, C. Piermarocchi, A. Quattropani, P. Schwendimann, *Phys. Rev. B* **53**, 13051 (1996).
15. Materials and methods are available as supporting material on *Science* Online.
16. J. R. Jensen, P. Borri, W. Langbein, J. M. Hvam, *Appl. Phys. Lett.* **76**, 3262 (2000).
17. P. Schwendimann, A. Quattropani, *Phys. Rev. B* **77**, 085317 (2008).

18. We thank C. B. Sørensen for growing the wafer and I. Akimov for discussions. This work was supported by the Deutsche Forschungsgemeinschaft research group "Quantum optics in semiconductor nanostructures." A patent application for the optical setup presented here is currently being filed.

Supporting Online Material

www.sciencemag.org/cgi/content/full/325/5938/297/DC1
Materials and Methods
SOM Text
References

3 April 2009; accepted 8 June 2009
10.1126/science.1174488

Band Formation from Coupled Quantum Dots Formed by a Nanoporous Network on a Copper Surface

Jorge Lobo-Checa,[1]*†‡ Manfred Matena,[1]† Kathrin Müller,[2] Jan Hugo Dil,[3,4] Fabian Meier,[3,4] Lutz H. Gade,[5] Thomas A. Jung,[2]‡ Meike Stöhr[1]‡

The properties of crystalline solids can to a large extent be derived from the scale and dimensionality of periodic arrays of coupled quantum systems such as atoms and molecules. Periodic quantum confinement in two dimensions has been elusive on surfaces, mainly because of the challenge to produce regular nanopatterned structures that can trap electronic states. We report that the two-dimensional free electron gas of the Cu(111) surface state can be trapped within the pores of an organic nanoporous network, which can be regarded as a regular array of quantum dots. Moreover, a shallow dispersive electronic band structure is formed, which is indicative of electronic coupling between neighboring pore states.

The electronic and optical properties of crystalline solids exhibit properties that derive to a large extent from the periodic arrangement and interactions of their component quantum systems, such as atoms or molecules. Extending the principle of such periodic coupling beyond the molecular regime has given rise to metamaterials, which are composed of regularly repeated units (*1*), in most cases, nanoparticles (*2*, *3*). Quantum effects that arise from confinement of electronic states have been extensively studied for surface states of noble metals, which are characterized by a quasi–two-dimensional (2D) electron gas. These may be visualized by scanning tunneling microscopy (STM) as standing wave patterns arising from scattering at steps and defects (*4*, *5*) or at large organic molecules (*6*). Examples of such surface state confinement comprise thin films (*7*), artificial nanoscale structures (*8*, *9*), vacancy and ad-atom islands (*10*, *11*), self-assembled 1D chains (*12*, *13*), vicinal surfaces (*14*–*16*), and quantum dots (*2*, *17*).

In spite of these previous examples, periodic quantum confinement in 2D at surfaces has always been elusive, mainly because of the difficulties encountered in the production of strictly regular nanopatterned structures that can trap electronic states. However, we note that Collier *et al*. observed coupling phenomena between quantum dots at a solid-liquid interface, namely between colloidal particles arranged in a Langmuir monolayer (*17*).

Periodic confinement in 2D is expected to induce regularly distributed discrete energy levels that could be experimentally observed through the appearance of nondispersive subbands, as previously reported for thin films (*7*) or 1D systems (*13*, *15*, *16*). The size of the confining entities embedded within the 2D periodic nanostructures should be larger than or comparable to a critical length of ~2 nm, as experimentally observed for 1D structures (*15*). The design of such structures is more readily achieved by using molecules as building blocks rather than atomic units, given the fundamental dimensions of these arrays. Potential candidates for molecular systems that might exhibit this zero-dimensional (0D) periodic electronic confinement are porous molecular surface networks. Their production is based on molecular self-assembly, which makes use of concepts established in supramolecular chemistry and has the advantage that identical parts are produced at once. This is in contrast, for instance, to assembly based on atom-by-atom positioning techniques (*8*, *9*). Self-assembled nanoporous networks have been obtained by using either hydrogen bonding motifs (*18*) or metal-complexation (*19*) on metal surfaces. Within the pores of these molecular nanoporous networks, electronic confinement is to be expected (*20*).

We report on the interplay of the surface state electrons of Cu(111) with a supramolecular porous network adsorbed on the Cu surface that leads to the formation of a 2D electronic band structure through the coupling of confined elec-

[1]Department of Physics, University of Basel, CH-4056 Basel, Switzerland. [2]Laboratory for Micro- and Nanotechnology, Paul Scherrer Institute, CH-5232 Villigen PSI, Switzerland. [3]Physik-Institut, Universität Zürich, Winterthurerstrasse 190, CH-8057 Zürich, Switzerland. [4]Swiss Light Source, Paul Scherrer Institute, CH-5232 Villigen, Switzerland. [5]Anorganisch-Chemisches Institut, Universität Heidelberg, Im Neuenheimer Feld 270, 69120 Heidelberg, Germany.

*Present address: Centre d'Investigaciò en Nanociència i Nanotecnologia (CIN2), 08193 Bellaterra (Barcelona), Spain.
†These authors contributed equally to this work.
‡To whom correspondence should be addressed. E-mail: jorge.lobo@cin2.es (J.L.-C.); thomas.jung@psi.ch (T.A.J.); meike.stoehr@unibas.ch (M.S.)